Fusion reactions in ^{6}Li + ^{90}Zr scattering

M. R. Cortes,[1,*] V. A. B. Zagatto,[1,†] J. L. Ferreira,[1,‡] J. Rangel,[1,2,§] L. F. Canto,[3,‖] and J. Lubian[1,¶]

[1]*Instituto de Física, Universidade Federal Fluminense, Avenida Litoranea s/n, Gragoatá, Niterói, 24210-340 Rio de Janeiro, Brazil*

[2]*Departamento de Matematica, Física e Computação Universidade do Estado do Rio de Janeiro, Faculdade de Tecnologia, Resende, 27537-000 Rio de Janeiro, Brazil*

[3]*Instituto de Física, Universidade Federal do Rio de Janeiro, CP 68528, 21941-972 Rio de Janeiro, Brazil*

(Received 7 August 2023; accepted 11 October 2023; published 7 November 2023)

We use a recently proposed theoretical model to evaluate complete and incomplete fusion cross sections in collisions of ^{6}Li with ^{90}Zr. The former is compared to the data of Kumawat *et al.* [H. Kumawat, V. Jha, V. V. Parkar, B. Roy, S. K. Pandit, R. Palit, P. K. Rath, C. F. Palshetkar, S. K. Sharma, S. Thakur, A. K. Mohanty, A. Chatterjee, and S. Kailas, Phys. Rev. C **86**, 024607 (2012)], while the theoretical cross section for the incomplete fusion of the deuteron in ^{6}Li is compared to a cross section extracted from inclusive α-production data. The overall agreement between theory and experiment is good. Additional validation of the procedure is obtained by applying it to the ^{6}Li + ^{59}Co reaction at energies above the Coulomb barrier.

DOI: 10.1103/PhysRevC.108.054601

I. INTRODUCTION

Fusion reactions induced by weakly bound projectiles are a subject of great interest in low-energy nuclear physics [1–5]. The low breakup threshold of the projectile affects fusion in two ways. First, it gives rise to a long tail in the projectile's density, leading to a lower Coulomb barrier. This is a static effect of the low breakup threshold, which enhances fusion at all collision energies. On the other hand, it also strongly influences the reaction dynamics. Owing to the strong couplings with the breakup channels, the projectile may dissociate as it approaches the target ($^{6}\mathrm{Li} \rightarrow d + \alpha$). Then, besides complete fusion (CF), where the whole projectile fuses with the target, there are the new processes of incomplete fusion (ICF), where one of the clusters fuses with the target, whereas the other does not. They are denoted by ICFd (fusion of the deuteron) and ICFα (fusion of the α). There is also the possibility that both fragments fuse sequentially with the target. This process cannot be experimentally distinguished from the usual complete fusion.

Measuring CF and ICF cross sections is a great challenge for experimentalists. Only for some particular projectile-target combinations is it possible to determine these cross sections by identifying the individual evaporation residues of the CF and/or ICF processes. This kind of data for ^{6}Li projectiles is available for the following targets: ^{209}Bi [6,7], ^{198}Pt [8], ^{197}Au [9], ^{159}Tb [10], ^{144,152,154}Sm [11–13], ^{124}Sn [14], ^{90}Zr [15], ^{64}Ni [16], ^{59}Co [17,18], and ^{28}Si [19]. Calculating individual CF and ICF cross sections is also a very hard task. However, many theoretical models have been proposed over the last few decades. The first theoretical approaches were based on classical physics or semiclassical approximations [6,20–25]. They were followed by more realistic theories involving quantum mechanics [26–37].

Recently, the theoretical model proposed by Rangel *et al.* [36] was used to study CF and ICF in collisions of ^{6}Li with the heavy targets ^{124}Sn, ^{197}Au, ^{198}Pt, and ^{209}Bi. The predictions of the model were shown to be in good agreement with the data in Refs. [38,39]. Comparing the CF cross section with predictions of barrier penetration models (BPMs) with a potential that neglects the low binding of the projectile, we found that the CF cross section was suppressed by ≈40% above the Coulomb barrier, and enhanced at sub-barrier energies. The model also predicted that the CF and ICF cross sections for these systems have comparable values above the barrier. Further, one found that the ICFα cross section is systematically lower than that for ICFd. Above the Coulomb barrier, the former is about 2/3 of the latter, and at sub-barrier energies, it is at least one order of magnitude lower. Nevertheless, it is not known whether these conclusions remain valid for lighter targets.

In the present paper, we carry out a similar study in collisions of ^{6}Li with a lighter target, ^{90}Zr. We perform CF and ICF calculations and compare our results to data from the experiments of Kumawat *et al.* [15,40]. Reference [15] reported CF data in collisions of ^{6}Li with ^{90}Zr, whereas Ref. [40] measured the total α-production cross section for the same system. Although the latter does not give directly any ICF cross section, we show that the ICFd cross section can be extracted from it. The procedure of extraction of the ICF cross section from the inclusive total α-production cross section is also applied to the ^{6}Li + ^{59}Co reaction measured in Ref. [18], which reports the

*mariane.cortess@gmail.com
†vzagatto@id.uff.br
‡jonas@if.uff.br
§jeannierangel@gmail.com
‖canto@if.ufrj.br
¶jlubian@id.uff.br

experimental angular distributions of protons, deuterium, and α particles acquired in singles mode.

The paper is organized as follows. In Sec. II, we give a brief description of our theoretical model. In Sec. III, we use the model to evaluate the CF, ICFd, and ICFα cross sections for the ^{6}Li + ^{90}Zr system and show how an ICFd cross section can be extracted from inclusive α-production data. The same procedure to determine the ICFd cross section from inclusive α-production data is used in Sec. IV for the ^{6}Li + ^{59}Co system. Finally, in Sec. V, we present the summary of our main results.

II. THE THEORETICAL MODEL

We use the theoretical model proposed by Rangel *et al.* [36], as described in detail in Ref. [38]. The main features of this model are briefly presented below.

The projectile is assumed to be formed by two clusters, c_1 and c_2, which in the case of ^{6}Li are the deuteron (d) and the α particle, respectively.

The real part of the projectile-target interaction is written as the sum of interactions between the two clusters and the target, namely,

$$V(\mathrm{R}, \mathbf{r}) = V_1(r_1) + V_2(r_2). \tag{1}$$

Above, r_1 and r_2 are the distances between the cluster c_1 and c_2 and the target, respectively. They are the moduli of the vectors $\mathbf{r}_1$ and $\mathbf{r}_2$, related to the projectile-target vector, $\mathbf{R}$, and to the vector between the clusters, $\mathbf{r}$, by the equations

$$\mathbf{r}_1 = \mathbf{R} + \tfrac{2}{3}\,\mathbf{r}, \quad \mathbf{r}_2 = \mathbf{R} - \tfrac{1}{3}\,\mathbf{r}.$$

The potentials of Eq. (1) contain a Coulomb and a nuclear term. In the present calculations, the latter is given by the São Paulo potential (SPP) [41,42] for the ^{2}H + ^{90}Zr and the ^{4}He + ^{90}Zr systems. The expectation value of the potential of Eq. (1) with respect to the ground state of the projectile, $\phi_0(\mathbf{r})$,

$$V_{00}(R) = \langle \phi_0 | V(\mathrm{R}, \mathbf{r}) | \phi_0 \rangle, \tag{2}$$

plays the role of the real part of the optical potential. The barrier parameters associated with this potential are

$$R_{\mathrm{B}}^{00} = 10.1\,\mathrm{fm}, \quad V_{\mathrm{B}}^{00} = 15.8\,\mathrm{MeV}, \quad \text{and} \quad \hbar\omega^{00} = 3.5\,\mathrm{MeV}. \tag{3}$$

Note that the barrier for this potential is lower than the one of the SPP, ignoring the cluster structure of the projectile. The barrier parameters for this potential, which we denote by $V_{\mathrm{PT}}(r)$, are

$$R_{\mathrm{B}}^{\mathrm{PT}} = 9.7\,\mathrm{fm}, \quad V_{\mathrm{B}}^{\mathrm{PT}} = 16.6\,\mathrm{MeV}, \quad \text{and} \quad \hbar\omega^{\mathrm{PT}} = 4.0\,\mathrm{MeV}. \tag{4}$$

We follow Ref. [38], adopting different imaginary potentials for bound and unbound channels. For the former, the imaginary potential $W_{\mathrm{B}}(R)$ is a short-range function depending only on the projectile-target distance, R. For the latter, the imaginary potential is the sum of short-range functions of the distance between each cluster and the target. That is,

$$W_{\mathrm{C}}(r_1, r_2) = W_1(r_1) + W_2(r_2). \tag{5}$$

The potential W_i accounts for the inclusive absorption of the cluster c_i.

One carries out the channel expansion of the full scattering wave function, distinguishing its components in the spaces of bound channels, Ψ_{B}, and in the continuum (breakup channels), Ψ_{C}, namely,

$$\Psi^{(+)} = \Psi_{\mathrm{B}} + \Psi_{\mathrm{C}}. \tag{6}$$

In the case of ^{6}Li, Ψ_{B} is just the elastic wave function. The breakup component of the wave function is approximated by a finite sum over discretized continuum channels (bins) by the continuum discretized coupled channel (CDCC) method [36,37].

The components of the wave function in the two subspaces, Ψ_{B} and Ψ_{C}, are calculated by the CDCC version of the FRESCO computer code [43]. These wave functions are used to evaluate the cross sections:

$$\sigma_{\mathrm{DCF}} = \frac{K}{E}\,\langle \Psi_{\mathrm{B}} |\, W_{\mathrm{B}} \,| \Psi_{\mathrm{B}} \rangle, \tag{7}$$

$$\sigma_{\mathrm{F}}^{(1)} = \frac{K}{E}\,\langle \Psi_{\mathrm{C}} |\, W_1 \,| \Psi_{\mathrm{C}} \rangle, \tag{8}$$

$$\sigma_{\mathrm{F}}^{(2)} = \frac{K}{E}\,\langle \Psi_{\mathrm{C}} |\, W_2 \,| \Psi_{\mathrm{C}} \rangle, \tag{9}$$

where E is the collision energy, and K is the corresponding wave number. Then, performing angular momentum expansions, these expressions can be written as

$$\sigma_{\mathrm{DCF}} = \frac{\pi}{K^2} \sum_{J=0}^{\infty} (2J+1)\, \mathcal{P}_J^{\mathrm{DCF}}, \tag{10}$$

$$\sigma_{\mathrm{F}}^{(1)} = \frac{\pi}{K^2} \sum_{J=0}^{\infty} (2J+1)\, \mathcal{P}_J^{(1)}, \tag{11}$$

$$\sigma_{\mathrm{F}}^{(2)} = \frac{\pi}{K^2} \sum_{J=0}^{\infty} (2J+1)\, \mathcal{P}_J^{(2)}. \tag{12}$$

Above, P_J^{DCF} is the probability of direct absorption of the projectile (without breakup), whereas $P_J^{(i)} (i = 1, 2)$ is the inclusive absorption probability of the cluster i (independently of what happens to the other cluster). The calculation of these probabilities is discussed in detail in the Appendix of Ref. [37].

However, the cross sections of Eqs. (10), (11), and (12) are not the cross sections observed in actual experiments. The available CF data correspond to the sum of contributions from the direct complete fusion (DCF) and sequential complete fusion (SCF) processes, which cannot be distinguished experimentally. Conversely, the experimental ICF cross sections are not inclusive data. They are exclusive cross sections corresponding to breakup events, followed by the capture of one of the clusters, with the other emerging from the interaction region. Therefore, quantum mechanical CDCC calculations on their own cannot describe the observable fusion cross section.

To make predictions of observable fusion cross sections, the theoretical models of Refs. [36–39] resort to assumptions based on classical probability theory. The ICF and the SCF

probabilities are derived from the inclusive capture probabilities $P_J^{(1)}$ and $P_J^{(2)}$ through the intuitive expressions

$$\mathcal{P}_J^{\mathrm{ICF1}} = P_J^{(1)} \times \left[1 - P_J^{(2)}\right], \tag{13}$$

$$\mathcal{P}_J^{\mathrm{ICF2}} = P_J^{(2)} \times \left[1 - P_J^{(1)}\right], \tag{14}$$

$$\mathcal{P}_J^{\mathrm{SCF}} = P_J^{(1)} \times P_J^{(2)}. \tag{15}$$

Using the above equations, one gets the ICF and SCF cross sections through the expressions

$$\sigma_{\mathrm{ICF}d} = \frac{\pi}{K^2} \sum_{J=0}^{\infty} (2J+1)\, \mathcal{P}_J^{\mathrm{ICF}d}\,, \tag{16}$$

$$\sigma_{\mathrm{ICF}\alpha} = \frac{\pi}{K^2} \sum_{J=0}^{\infty} (2J+1)\, \mathcal{P}_J^{\mathrm{ICF}\alpha}, \tag{17}$$

$$\sigma_{\mathrm{SCF}} = \frac{\pi}{K^2} \sum_{J=0}^{\infty} (2J+1)\, \mathcal{P}_J^{\mathrm{SCF}}. \tag{18}$$

Above, we changed the notation to indicate that c_1 and c_2 are respectively the d and the α particle.

The CF cross section is then given by the equation

$$\sigma_{\mathrm{CF}} = \sigma_{\mathrm{DCF}} + \sigma_{\mathrm{SCF}}, \tag{19}$$

where σ_{DCF} and σ_{SCF} are given by Eqs. (10) and (18), respectively.

One can also define the total fusion (TF) cross section:

$$\sigma_{\mathrm{TF}} = \sigma_{\mathrm{CF}} + \sigma_{\mathrm{ICF}} \equiv \sigma_{\mathrm{CF}} + \sigma_{\mathrm{ICF}d} + \sigma_{\mathrm{ICF}\alpha}. \tag{20}$$

III. FUSION REACTIONS IN ^{6}Li - ^{90}Zr COLLISIONS

A. Complete fusion

Kumawat *et al.* [15] measured the CF cross section for the ^{6}Li + ^{90}Zr system by detecting delayed characteristic γ rays emitted by the evaporation residues. However, evaporation residues with short half-lives cannot be detected by this method. Furthermore, the experiment also misses evaporation residues that decay by the emission of an α particle. To deal with this situation, the contribution of such decay modes to the CF cross section was estimated by the CASCADE [44] statistical code. Then, to some extent, these data are model dependent. Note that similar procedures are used in other experimental works (see, e.g., Refs. [16,17,19,45]).

Figure 1 shows a comparison between the CF data of Kumawat *et al.* [15] and the CF cross section predicted by our model. One observes that the theoretical curve lies slightly above the data points at energies just above the barrier. However, if one considers that the theoretical model has no free parameter, the agreement between theory and experiment is fairly good.

The figure also shows the cross section of the BPM with the potential $V_{\mathrm{PT}}(r)$. Comparing the CF cross sections with the one predicted by the BPM, one finds a slight enhancement at sub-barrier energies and a suppression of ≈40% above the Coulomb barrier.

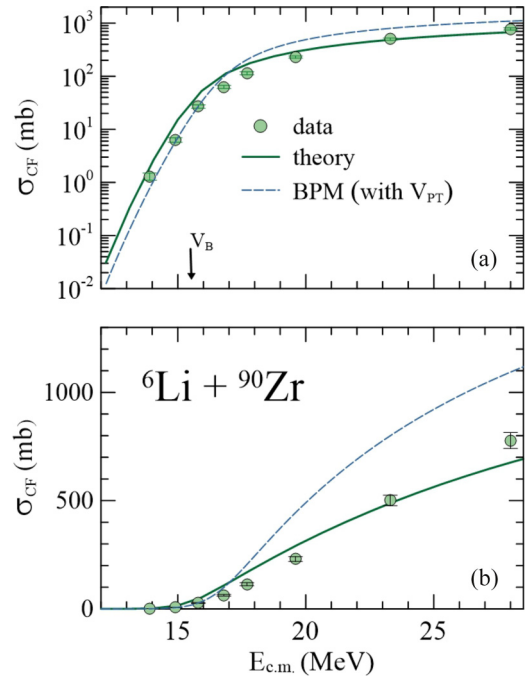

FIG. 1. The experimental CF cross section of Kumawat *et al.* [15], in comparison with the cross section predicted by the theoretical model, and by the barrier penetration model.

B. Total fusion and incomplete fusion

ICF and TF cross sections have not been measured for this system. However, one can extract some experimental information about these cross sections from the inclusive α-particle production cross section, $\sigma_\alpha^{\mathrm{inc}}$, measured in 2010 by the same group [40]. This cross section is the sum of cross sections associated with several reaction mechanisms. One can write

$$\sigma_\alpha^{\mathrm{inc}} = \sigma_\alpha^{\mathrm{EBU}} + \sigma_\alpha^{1n} + \sigma_\alpha^{1p} + \sigma_\alpha^{\mathrm{CF}} + \sigma_{\mathrm{ICF}d}. \tag{21}$$

In the above equation, we used the following notation:

$\sigma_\alpha^{\mathrm{EBU}}$ = elastic breakup cross section
(^{6}Li + ^{90}Zr → ^{2}H + ^{4}He + ^{90}Zr),

σ_α^{1n} = neutron stripping cross section
(^{6}Li + ^{90}Zr → ^{5}Li + ^{91}Zr → p + ^{4}He + ^{91}Zr),

σ_α^{1p} = proton stripping cross section
(^{6}Li + ^{90}Zr → ^{5}He + ^{91}Nb → n + ^{4}He + ^{91}Nb),

$\sigma_\alpha^{\mathrm{CF}}$ = CF + evaporation of an α particle
(^{6}Li + ^{90}Zr → ^{96}Nd → $(1n, 2n, 3n), \alpha$).

In principle, one should also consider the cross section for the direct transfer of the d cluster in ^{6}Li. However, considering the optimal Q value of this reaction, one would expect that it populates highly excited states in ^{92}Nb. This would characterize transfer to the continuum, which has already been considered in $\sigma_\alpha^{\mathrm{EBU}}$.

TABLE I. The experimental inclusive α-production cross sections [40] used to determine $\sigma_{\mathrm{ICF}d}$. The other cross sections on the right-hand side of Eq. (22), determined as described in the text, are shown in columns 3, 4, 5, and 6.

$E_{\mathrm{c.m.}}$ (MeV)	$\sigma_\alpha^{\mathrm{inc}}$ (mb)	$\sigma_\alpha^{\mathrm{CF}}$ (mb)	σ^{EBU} (mb)	σ_α^{1n} (mb)	σ_α^{1p} (mb)
13.9	32 ± 19	0.01	8.5	2.0	0.3
15.8	122 ± 10	1.3	12.9	14.1	0.7
17.7	274 ± 15	16.2	17.9	27.5	1.1
19.6	360 ± 20	37.6	24.4	30.9	1.3
23.3	460 ± 30	94.2	35	29.5	1.5
28.0	540 ± 86	172	45.3	26.9	1.5

If inclusive α-production data are available and one evaluates the $\sigma_\alpha^{\mathrm{EBU}}$, σ_α^{1n}, σ_α^{1p}, and $\sigma_\alpha^{\mathrm{CF}}$ cross sections, $\sigma_{\mathrm{CF}d}$ can be determined by the relation

$$\sigma_{\mathrm{ICF}d} = \sigma_\alpha^{\mathrm{inc}} - \left\{\sigma_\alpha^{\mathrm{EBU}} + \sigma_\alpha^{1n} + \sigma_\alpha^{1p} + \sigma_\alpha^{\mathrm{CF}}\right\}. \quad (22)$$

Note that this procedure introduces some model dependence in the ICFd data.

A similar procedure was used in the theoretical work of Lei and Moro [35]. These authors proposed to evaluate the CF cross section by subtracting the contribution from direct reactions from the total reaction cross section, that is, inelastic scattering, elastic breakup (EBU), and nonelastic breakup processes, where one of the projectile's clusters emerges from the interaction region. CF cross sections for the $^{6,7}\mathrm{Li} + {}^{209}\mathrm{Bi}$ systems calculated by this method were shown to be in very good agreement with the data of Dasgupta *et al.* [7].

We determined the ICFd cross section for the $^{6}\mathrm{Li} + {}^{90}\mathrm{Zr}$ system by using the inclusive α-production data of Ref. [40], and performing realistic calculations of the remaining cross section on the right-hand side of Eq. (22).

The EBU cross section was obtained by running the CDCC version of the FRESCO code also used to generate the wave functions required to evaluate the CF and ICF cross sections of the theoretical model, through the expressions given in the Appendix of Ref. [37].

The contribution from the α-decay modes of ^{96}Tc and its lighter isotope produced by neutron evaporation was obtained by Monte Carlo calculations performed with the code PACE4 [46,47]. We ran the code giving as input the experimental fusion cross section of Ref. [15].

To determine σ_α^{1n} and σ_α^{1p}, we performed realistic coupled reaction channel (CRC) calculations. We carried out separate structural calculations using the NUSHELLX code [48], which allows us to consider all the couplings between the states of the initial and final partitions, as well as all the (l, s, j) combinations of the overlap functions between each pair of states. The details of these calculations can be found in the Appendix.

The experimental α-production cross section of Ref. [40] is shown in Table I, together with the other cross sections used to determine $\sigma_{\mathrm{ICF}d}$. Note that the values of $\sigma_\alpha^{\mathrm{CF}}$ in the table are somewhat different from the ones given in Ref. [40]. Although they were obtained by different statistical model codes (we used PACE4, whereas Kumawat *et al.* used CASCADE), the difference must be mainly because we used as an input the experimental CF cross section measured by Kumawat *et al.* [15] in 2012, which was not available at that time. The σ_α^{1n} and σ_α^{1p} cross sections in the table are also significantly different from the ones given in Ref. [40], where they were estimated within the distorted wave Born approximation.

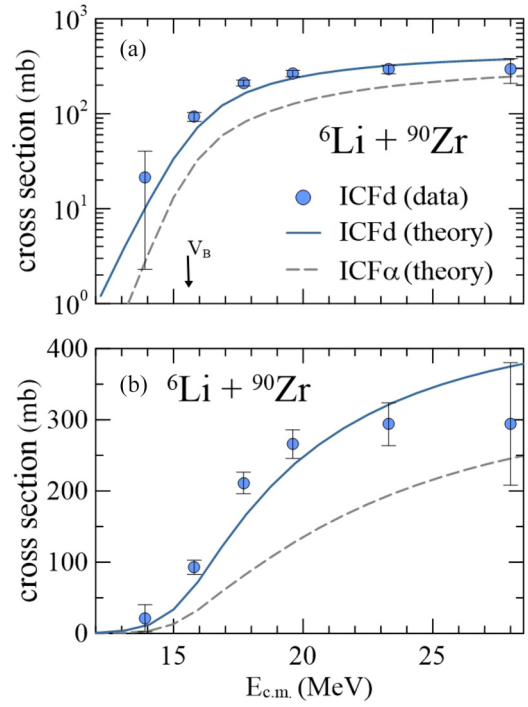

FIG. 2. The ICFd cross section determined from the inclusive α-production data of Kumawat *et al.* [15], in comparison with the prediction of the theoretical model.

Figure 2 shows the ICFd cross section extracted from the α-production data (solid circles) in comparison with the $\sigma_{\mathrm{ICF}d}$ cross section predicted by our theoretical model (blue solid line). The results are shown in logarithmic [Fig. 3(a)] and linear [Fig. 3(b)] scales. One concludes that the overall agreement between theory and experiment is good. The figure also shows the theoretical ICFα cross section, which is

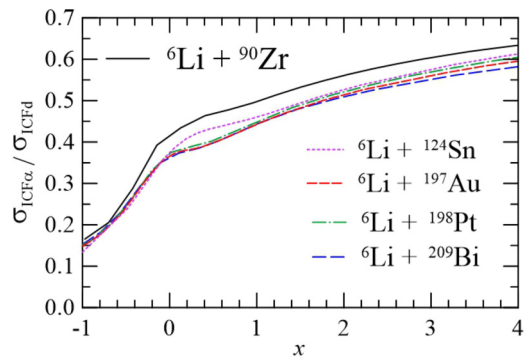

FIG. 3. The ratio $\mathcal{R} = \mathrm{ICF}\alpha/\mathrm{ICF}d$ for the $^{6}\mathrm{Li} + {}^{90}\mathrm{Zr}$ system and for the heavier systems studied in Ref. [38].

systematically lower than $\sigma_{\mathrm{ICF}d}$. This cross section cannot be related to the inclusive α-production data of Ref. [40].

The relative importance of the two ICF cross sections predicted by the theoretical model is investigated in Fig. 3. The figure shows the ratio $\mathcal{R} = \mathrm{ICF}\alpha/\mathrm{ICF}d$ for the ^{6}Li + ^{90}Zr system, and also for collisions of ^{6}Li with the heavier targets ^{124}Sn, ^{197}Au, ^{198}Pt, and ^{209}Bi [38]. The results are shown as functions of the reduced energy variable [49,50],

$$x = \frac{E - V_{\mathrm{B}}}{\hbar\omega},$$

where V_{B} and $\hbar\omega$ are the barrier parameters associated with the potential V_{00} of Eq. (2). One notices that the ratios for the five systems are very similar, and they grow with the collision energy. They are about 0.15 for $x = -1$ ($E = V_{\mathrm{B}} - \hbar\omega$) and $\approx$0.6 for $x = 4$ ($E = V_{\mathrm{B}} + 4\,\hbar\omega$). As the system mass increases, the ratio moves slightly down. These trends cannot be checked experimentally. Very few experiments measure both $\sigma_{\mathrm{ICF}\alpha}$ and $\sigma_{\mathrm{ICF}d}$, and the ones that do find different trends. These two cross sections are available in collisions of ^{6}Li with ^{124}Sn [14] and ^{197}Au [9]. In the former case, $\sigma_{\mathrm{ICF}\alpha}$ is systematically lower than $\sigma_{\mathrm{ICF}d}$, but the ratio is much smaller than the one predicted by the theoretical model. In the latter case, $\sigma_{\mathrm{ICF}\alpha}$ is lower than $\sigma_{\mathrm{ICF}d}$ around and below the Coulomb barrier. However, the ratio becomes larger than 1 at higher energies.

Now we discuss the TF cross section. Although experimental values of this cross section are not available, we can determine the "partial" TF cross section:

$$\overline{\sigma}_{\mathrm{TF}} = \sigma_{\mathrm{TF}} - \sigma_{\mathrm{ICF}\alpha} \equiv \sigma_{\mathrm{CF}} + \sigma_{\mathrm{ICF}d}.$$

Figure 4 shows the experimental $\overline{\sigma}_{\mathrm{TF}}$, in comparison to the corresponding cross section predicted by the theoretical model. The agreement between experiment and theory is very good, at all collision energies. The figure also shows the full TF cross section (also including $\sigma_{\mathrm{ICF}\alpha}$) predicted by the model, as a dashed line. Then, the difference between the dashed and the solid lines corresponds to the contribution from the ICFα process, according to the theoretical model.

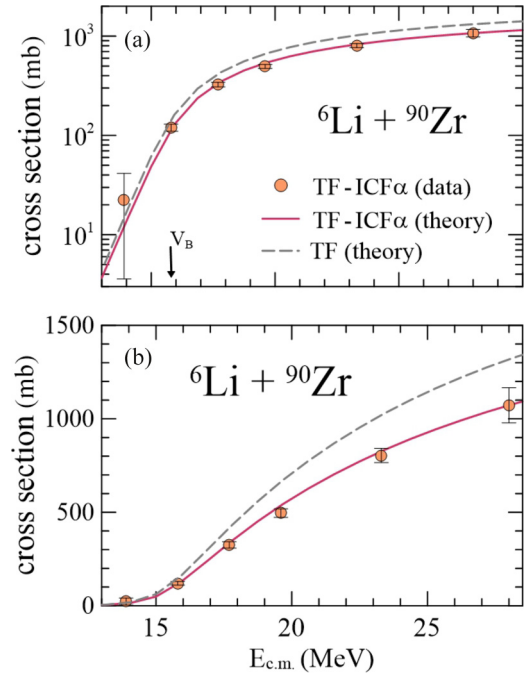

FIG. 4. The theoretical $\overline{\sigma}_{\mathrm{TF}}$ cross section, in comparison to the one extracted from the α-production data of Kumawat *et al.* [40]. The total fusion cross section of our model, including the contribution of ICFα, is also shown (black dashed line).

IV. ICF*d* CROSS SECTION IN ^{6}Li - ^{59}Co COLLISIONS

Now we use a similar procedure to extract ICF data from inclusive α-particle measurements for the ^{6}Li + ^{59}Co system. In Ref. [18], the angular distributions of protons, deuterium, and α particles acquired in singles mode were reported. The experiment was carried out at four different bombarding energies: $E_{\mathrm{lab}} = 17.4$, 21.5, 25.5, and 29.6 MeV. The integrated cross sections of deuterium and α particles can be found in Table 1 of Ref. [18]. In contrast to the data for the ^{6}Li + ^{90}Zr reaction presented in Ref. [40], the cross sections in the referenced table already provide the information without considering the contribution of the CF cross sections [18,51–53] to the α angular distributions. Therefore, the remaining contribution of the scattered particles comes from ICF, BU, and transfers.

Reference [18] also brings a detailed discussion of the CDCC calculations performed to incorporate the expected contributions from the BU process. Both sets of information were directly extracted from Table 1 of Ref. [18] and were used in our subsequent analysis. To derive the ICF*d* cross sections, one should subtract the transfer contributions that could lead to the production of α particles.

Due to their high Q and Q_{opt} values, it is expected that the deuterium-transfer channel populates the continuum states of the recoiling ^{61}Ni, which is formally equivalent to the BU process already considered in the CDCC calculations. The remaining transfer processes that may generate α particles are, once again, the one-neutron (leading to ^{5}Li) and one-proton (^{5}He) stripping reactions, both of which decay into ^{4}He. Both processes have been calculated using the CRC method. A complete description of both calculations can be found in the Appendix. Table II summarizes the information necessary to obtain the ICF*d* cross sections.

From Fig. 5, it is evident that the theoretical cross section overestimates the data, although they remain compatible within the uncertainties. This trend is also observed in the case

TABLE II. α-particle cross sections from Ref. [40] (already disregarding the fusion cross section), and the estimates for the BU (from Table 1 of Ref. [40]), one-neutron, and one-proton transfer cross sections for each bombarding energy.

E_{lab} (MeV)	$\sigma^{\alpha}_{\mathrm{expt.}}$ (mb)	σ_{BU} (mb)	σ_{1n} (mb)	σ_{1n} (mb)
17.4	243(36)	33.6	11.4	0.18
21.5	319(38)	44.9	10.8	0.25
25.5	332(33)	54.7	10.3	0.29
29.6	322(23)	61.2	9.8	0.31

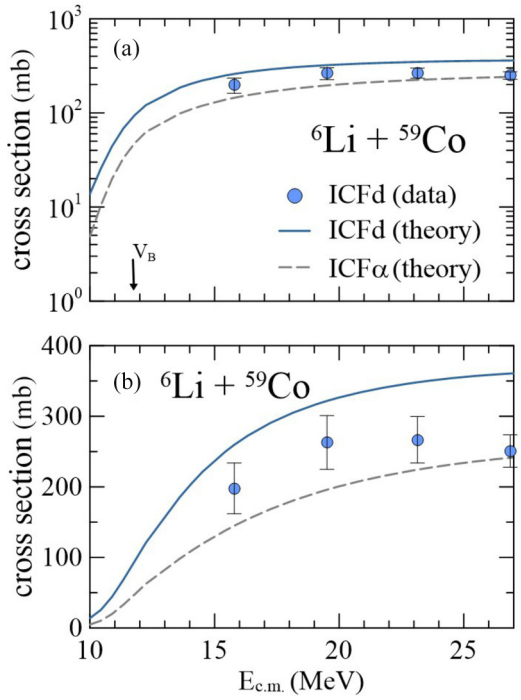

FIG. 5. Comparison of deuterium ICF data points (extracted from α-particle angular distributions) with the theoretical lines of ICF_α and d ICF_d.

of ^{6}Li + ^{90}Zr for data above the Coulomb barrier, suggesting a potential issue in this energy region for both systems. It is important to note that the experimental data points were derived from α-particle distributions obtained from Refs. [18,40], with estimated contributions subtracting the CF, BU, and transfer cross sections. After the cross sections for these channels are subtracted, it is inferred that the remaining α particles are exclusively originated from the ICF of deuteron. However, at higher bombarding energies, this assumption may not be valid. When one of the fragments fuses with the target, it generates reaction products that can also subsequently decay by emitting particles. These secondary evaporated particles may include α particles, which are present in the experimentally acquired α distributions, or protons, which have not being considered. Consequently, a portion of the experimental ICFd cross sections was not accounted for in the α distributions.

To estimate the cross sections of the evaporated particles, we performed calculations with the remaining kinetic energy (subtracting the α-deuteron binding energy in ^{6}Li), using the PACE4 code [46,47]. In the case of ^{6}Li + ^{90}Zr, the upper limit of the proton evaporation cross section for the ICFd is approximately 2% of the experimental cross section for the lowest bombarding energy. However, for the highest energy point, this missing contribution could be as high as 18%. This clarifies why we succeeded in describing the ICFd in the previous section. Since the data for ^{6}Li + ^{59}Co were obtained at energies significantly above the Coulomb barrier, it is expected that this effect would be more pronounced in this case. Further PACE4 estimations revealed that the contribution of proton evaporation could represent values ranging from 20 to 45% of the ICFd. This is the reason for the theoretical overestimation of the experimental ICFd cross section observed in Fig. 5.

V. SUMMARY

We investigated the fusion processes taking place in collisions of ^{6}Li on ^{90}Zr. For this purpose, we used a recently developed theoretical model [36–38] to calculate the CF, ICFd, and ICFα cross sections. The theoretical CF cross section was shown to be in good agreement with the data of Kumawat *et al.* [15].

Although there are no ICF or TF data for this system, we extracted experimental information on the ICFd cross section by subtracting from the inclusive α-production data [40] the contributions from all other processes that lead to an α particle in the exit channel. The ICFd cross section obtained in this way was compared with the one predicted by the theoretical model, and the agreement was good.

We found that the main features of the fusion cross sections in the ^{6}Li + ^{90}Zr system are similar to the ones found in collisions of ^{6}Li with heavier targets [38,39], namely, the following.

(1) Comparing the CF cross section with predictions of the barrier penetration model with the potential $V_{\mathrm{PT}}(r)$, one finds enhancement at sub-barrier energies and suppression of $\approx$40% above the Coulomb barrier.

(2) The CF and ICF cross sections at above-barrier energies are of the same order.

(3) The ICFα cross section is always lower than the ICFd one, and the ratio $\mathcal{R} = \sigma_{\mathrm{ICF}\alpha}/\sigma_{\mathrm{ICF}d}$ increases monotonically with the collision energy.

The first two of these trends have been confirmed experimentally. On the other hand, the relative importance of the ICFα and ICFd contributions to the ICF cross section is still unclear because there are very scarce data on them. Further measurements of ICFd and ICFα cross sections are called for.

The same procedure was used to extract the ICFd cross section from the inclusive α-production data [18] of the ^{6}Li + ^{59}Co system. In this case, the theoretical cross section slightly overpredicted the experimental data. The reason for this overprediction might be attributed to some contribution of proton evaporation to the ICFd in this energy regime.

ACKNOWLEDGMENTS

This work was supported in part by the Brazilian funding agencies CNPq, FAPERJ, CAPES, and Instituto Nacional de Ciência e Tecnologia- Física Nuclear e Aplicações (Project No. 464898/2014-5).

APPENDIX: CALCULATION OF THE N- AND P-STRIPPING CROSS SECTIONS

In this Appendix, we give some details of the CRC calculations performed in the present paper to derive the transfer cross section that contributes to the inclusive α cross section reported in Refs. [18,40].

1. ^{6}Li + ^{90}Zr

To derive spectroscopic amplitudes for the target overlaps the NUSHELLX code [48] was used. The structural calculations considered a model space consisting of the $1f_{5/2}$, $2p_{3/2}$, $2p_{1/2}$, $1g_{9/2}$, $1g_{7/2}$, $2d_{5/2}$, $2d_{3/2}$, and $3s_{1/2}$ orbitals, using the *snt* interaction available in the NUSHELLX program. This particular interaction is one of the few available that allow for the simultaneous description of the structures of ^{90}Zr, ^{91}Zr (one-neutron transfer recoil), and ^{91}Nb (one-proton transfer recoil) nuclei.

The ^{90}Zr is composed of 40 protons and the magic number of 50 neutrons, so it is expected that the neutron excitations will predominantly occur in high-lying excited states, while the proton excitations should well describe the low-lying states. Due to the large model space used, certain restrictions were imposed to make the structural calculations computationally feasible. These restrictions involved treating the core as inert and allowing a reduced number of valence particles to describe the structure of the nuclei under investigation. To describe the structure of ^{90}Zr, both ^{86}Sr and ^{82}Kr cores were employed, yielding similar results in terms of the ordering and excitation energies of states. However, using a ^{86}Sr core was preferred due to its lower computational demand. Attempts were also made with a ^{76}Se core, but the calculations did not converge. The spin parity, excitation energies, and ordering of states in ^{90}Zr, ^{91}Zr, and ^{91}Nb were well described, except for the inversion of the ground state and first excited state in the case of ^{91}Nb. This inversion of these states, energetically separated by only 104 keV, indicates no significant calculation issues.

Before performing CRC calculations to obtain the transfer cross sections relevant to this paper, it is crucial to properly describe the elastic channel of the ^{6}Li + ^{90}Zr reaction. ^{6}Li is known for being weakly bound and easily breaking up with a low excitation energy of 1.474 MeV. This characteristic leads to several reaction channels strongly connected to the elastic channel. An accurate description of the elastic channel is essential for properly understanding the transfer channel, as studied in Ref. [54]. Several attempts have been made to describe the elastic channel. The one that resulted in the best agreement with data was the coupled channel (CC) calculations, including the 0^{+} (ground state), 0^{+} ($E^{\star} = 1.760$ MeV), 2^{+} ($E^{\star} = 2.186$ MeV), 5^{-} ($E^{\star} = 2.319$ MeV), and 3^{-} ($E^{\star} = 2.748$ MeV) states of the target nucleus. The reduced electric transition probability values used in the calculations were taken from Refs. [55,56]. Concerning the potential adopted, we have used the optical potential proposed in Ref. [54].The optical model calculations using this potential were found to be very similar to the CC calculations that included the states mentioned above, employing the same potential. This indicates that the coupling of these states with the elastic channel is not significant. With a well-established potential for the entrance partition, one can proceed with the CRC calculations, which include the transfer channels.

A prior representation with a complex remnant was employed in the CRC calculations performed in this paper. This choice was based on the well-established fact that the optical potential could describe the elastic data. The valence particle interaction was modeled for both transfer cases using a real Woods-Saxon (WS) potential with adjustable depth to reproduce the valence-core binding energy. Usual parameters for reduced radius ($r_o = 1.25$ fm) and diffuseness ($a = 0.60$ fm) were considered. A spin-orbit interaction with the same parameters was also used for the ejectile-valence interaction.

In the case of one-neutron stripping, with a Q value of 1.531 MeV, the expected excitation energy of the recoiling nucleus is of the same order of magnitude. Therefore, all excited states up to $E^{\star} = 2.5$ MeV in ^{91}Zr were included in the coupling scheme. The description of a one-proton transfer is more challenging. Its Q value is -0.807 MeV, resulting in the fact that the minimum expected excitation energy for the recoil nucleus is close to 5 MeV. Considering that ^{91}Nb has a proton separation energy of 5.1 MeV, it is expected that the transferred proton may populate the continuum states of this nucleus. Another difficulty in studying ^{91}Nb is its high state density, with many excited states with spin-parity assignments still unknown. Thus, the CRC calculations performed in this paper considered all the known states of ^{91}Nb, including $9/2^{+}$ (ground state), $1/2^{-}$ ($E^{\star} = 0.104$ MeV), $5/2^{-}$ ($E^{\star} = 1.187$ MeV), $3/2^{-}$ ($E^{\star} = 1.313$ MeV), $3/2^{-}$ ($E^{\star} = 1.613$ MeV), $1/2^{+}$ ($E^{\star} = 4.164$ MeV), and $1/2^{+}$ ($E^{\star} = 4.441$ MeV), as well as a discretization of the continuum. For that, the binning method was used. The continuum bins covered an excitation energy range of 5.1 to 10 MeV for ^{91}Nb with a width of 1 MeV. The proton-^{90}Zr relative angular momentum bins were considered up to $l = 5\hbar$.

2. ^{6}Li + ^{59}Co

Structural calculations have been performed using the NUSHELLX code, while the CRC calculations have been carried out using the FRESCO code. To obtain the wave functions that describe the single-particle states coupling the initial and final states of the transfer, a different model space (as well as a different interaction) compared to the ^{6}Li + ^{90}Zr reaction should be adopted. Reference [57] describes transfers between nickel isotopes, and since ^{59}Co is in the same mass region, it is natural to use the same orbitals/interaction in the present case. The model space considered here allows protons to populate the $1f_{7/2}$ and $2p_{3/2}$ orbitals, while neutrons can populate the $2p_{3/2}$, $1f_{5/2}$, $2p_{1/2}$, and $1g_{9/2}$ orbitals. One may notice the inversion of the first two neutron orbitals in ^{59}Co concerning ^{90}Zr, a crucial aspect considered in the present model space to describe the ^{59,60}Co and ^{60}Ni nuclear levels accurately. Such inversion does not play a key role in the ^{90}Zr case since the $2p_{3/2}$ and $1f_{5/2}$ orbitals are compressed within the core adopted. A ^{48}Ca core is used in the present model. The interaction used is described in Ref. [58], originally developed to describe the nuclear structure of nickel isotopes. Except for the inversion of the first two states of ^{60}Co (5^{+} and 2^{+}), the calculations properly describe all the low-lying states of the three previously mentioned nuclei. Since these states are separated by just 60 keV, this inversion has little significance for the present case.

As we did in the ^{6}Li + ^{90}Zr reaction before performing the CRC calculations, we conducted a study of the description

of the elastic channel of the ^{6}Li + ^{59}Co reaction to verify if the chosen optical potential was adequate. Using the elastic angular distributions from Ref. [51], it was once again verified that the optical potential proposed in Ref. [54] best described the data and was adopted. The São Paulo systematic has been adopted to describe the transfer partition and the same ingredients as in the previous calculations (i.e., prior representation with a complex remnant, valence particle interactions described as a WS potential) have been adopted again. Finally, the states chosen to be included in the coupling scheme were decided by properly studying the most probable excitation energy for the one-neutron and one-proton transfer processes. In the one-neutron stripping process, its Q value of 1.829 MeV indicates that the excited states of ^{60}Co should range in the same region; therefore, all the 25 known states up to $E^{\star} = 2.3$ MeV of ^{60}Co have been considered in the calculations. Studying the contributions of the most excited states, it was observed that including more states in the scheme would not significantly change the obtained results. Concerning the one-proton transfer, its high Q (4.944 MeV) and Q_{optimum} values indicate that only the continuum states (above the proton threshold energy) of ^{60}Ni should be populated. Since ^{60}Ni is an even-even nucleus, its bounded states are more separated from each other than those of the ^{91}Zr. Thus, only the first four states of ^{60}Ni (0^{+} g.s.; 2^{+} $E^{\star} = 1.3$ MeV; 2^{+} $E^{\star} = 2.2$ MeV; and 0^{+} $E^{\star} = 2.3$ MeV) plus a continuum discretization (from 10 to 15 MeV) have been considered. As in the previous case, the continuum bins had a 1-MeV width, and the relative angular momentum between the proton and ^{59}Co was considered up to $l = 5\hbar$.

[1] L. F. Canto, P. R. S. Gomes, R. Donangelo, and M. S. Hussein, Phys. Rep. **424**, 1 (2006).
[2] N. Keeley, R. Raabe, N. Alamanos, and J. L. Sida, Prog. Part. Nucl. Phys. **59**, 579 (2007).
[3] N. Keeley, N. Alamanos, K. W. Kemper, and K. Rusek, Prog. Part. Nucl. Phys. **63**, 396 (2009).
[4] L. F. Canto, P. R. S. Gomes, R. Donangelo, J. Lubian, and M. S. Hussein, Phys. Rep. **596**, 1 (2015).
[5] J. J. Kolata, V. Guimarães, and E. F. Aguilera, Eur. Phys. J. A **52**, 123 (2016).
[6] M. Dasgupta, D. J. Hinde, K. Hagino, S. B. Moraes, P. R. S. Gomes, R. M. Anjos, R. D. Butt, A. C. Berriman, N. Carlin, C. R. Morton *et al.*, Phys. Rev. C **66**, 041602(R) (2002).
[7] M. Dasgupta, P. R. S. Gomes, D. J. Hinde, S. B. Moraes, R. M. Anjos, A. C. Berriman, R. D. Butt, N. Carlin, J. Lubian, C. R. Morton *et al.*, Phys. Rev. C **70**, 024606 (2004).
[8] A. Shrivastava, A. Navin, A. Lemasson, K. Ramachandran, V. Nanal, M. Rejmund, K. Hagino, T. Ichikawa, S. Bhattacharyya, A. Chatterjee, S. Kailas, K. Mahata, V. V. Parkar, R. G. Pillay, and P. C. Rout, Phys. Rev. Lett. **103**, 232702 (2009).
[9] C. S. Palshetkar, S. Thakur, V. Nanal, A. Shrivastava, N. Dokania, V. Singh, V. V. Parkar, P. C. Rout, R. Palit, R. G. Pillay, S. Bhattacharyya, A. Chatterjee, S. Santra, K. Ramachandran, and N. L. Singh, Phys. Rev. C **89**, 024607 (2014).
[10] M. K. Pradhan, A. Mukherjee, P. Basu, A. Goswami, R. Kshetri, R. Palit, V. V. Parkar, M. Ray, S. Roy, P. R. Chowdhury, M. S. Sarkar, and S. Santra, Phys. Rev. C **83**, 064606 (2011).
[11] P. K. Rath, S. Santra, N. L. Singh, R. Tripathi, V. V. Parkar, B. K. Nayak, K. Mahata, R. Palit, S. Kumar, S. Mukherjee *et al.*, Phys. Rev. C **79**, 051601(R) (2009).
[12] P. K. Rath, S. Santra, N. L. Singh, K. Mahata, R. Palit, B. K. Nayak, K. Ramachandran, V. V. Parkar, R. Tripathi, S. K. Pandit *et al.*, Nucl. Phys. A **874**, 14 (2012).
[13] C. L. Guo, G. L. Zhang, S. P. Hu, J. C. Yang, H. Q. Zhang, P. R. S. Gomes, J. Lubian, X. G. Wu, J. Zhong, C. Y. He *et al.*, Phys. Rev. C **92**, 014615 (2015).
[14] V. V. Parkar, S. K. Sharma, R. Palit, S. Upadhyaya, A. Shrivastava, S. K. Pandit, K. Mahata, V. Jha, S. Santra, K. Ramachandran *et al.*, Phys. Rev. C **97**, 014607 (2018).
[15] H. Kumawat, V. Jha, V. V. Parkar, B. J. Roy, S. K. Pandit, R. Palit, P. K. Rath, C. S. Palshetkar, S. K. Sharma, S. Thakur, A. K. Mohanty, A. Chatterjee, and S. Kailas, Phys. Rev. C **86**, 024607 (2012).
[16] M. M. Moin Shaikh, S. Roy, S. Rajbanshi, M. K. Pradhan, A. Mukherjee, P. Basu, S. Pal, V. Nanal, R. G. Pillay, and A. Shrivastava, Phys. Rev. C **90**, 024615 (2014).
[17] C. Beck, F. A. Souza, N. Rowley, S. J. Sanders, N. Aissaoui, E. E. Alonso, P. Bednarczyk, N. Carlin, S. Courtin, A. Diaz-Torres *et al.*, Phys. Rev. C **67**, 054602 (2003).
[18] F. A. Souza, C. Beck, N. Carlin, N. Keeley, R. Liguori Neto, M. M. de Moura, M. G. Munhoz, M. G. Del Santo, A. A. P. Suaide, E. M. A. Szanto *et al.*, Nucl. Phys. A **821**, 36 (2009).
[19] M. Sinha and J. Lubian, Eur. Phys. J. A **53**, 224 (2017).
[20] K. Hagino, M. Dasgupta, and D. J. Hinde, Nucl. Phys. A **738**, 475 (2004).
[21] A. Diaz-Torres, D. J. Hinde, J. A. Tostevin, M. Dasgupta, and L. R. Gasques, Phys. Rev. Lett. **98**, 152701 (2007).
[22] A. Diaz-Torres, J. Phys. G **37**, 075109 (2010).
[23] A. Diaz-Torres, Comput. Phys. Commun. **182**, 1100 (2011).
[24] H. D. Marta, L. F. Canto, and R. Donangelo, Phys. Rev. C **89**, 034625 (2014).
[25] G. D. Kolinger, L. F. Canto, R. Donangelo, and S. R. Souza, Phys. Rev. C **98**, 044604 (2018).
[26] K. Hagino, A. Vitturi, C. H. Dasso, and S. M. Lenzi, Phys. Rev. C **61**, 037602 (2000).
[27] N. Keeley, K. W. Kemper, and K. Rusek, Phys. Rev. C **65**, 014601 (2001).
[28] A. Diaz-Torres and I. J. Thompson, Phys. Rev. C **65**, 024606 (2002).
[29] A. Diaz-Torres, I. J. Thompson, and C. Beck, Phys. Rev. C **68**, 044607 (2003).
[30] S. Hashimoto, K. Ogata, S. Chiba, and M. Yahiro, Prog. Theor. Phys. **122**, 1291 (2009).
[31] M. Boselli and A. Diaz-Torres, J. Phys. G **41**, 094001 (2014).
[32] M. Boselli and A. Diaz-Torres, Phys. Rev. C **92**, 044610 (2015).
[33] P. Descouvemont, T. Druet, L. F. Canto, and M. S. Hussein, Phys. Rev. C **91**, 024606 (2015).
[34] V. V. Parkar, V. Jha, and S. Kailas, Phys. Rev. C **94**, 024609 (2016).
[35] J. Lei and A. M. Moro, Phys. Rev. Lett. **122**, 042503 (2019).
[36] J. Rangel, M. Cortes, J. Lubian, and L. F. Canto, Phys. Lett. B **803**, 135337 (2020).

[37] M. R. Cortes, J. Rangel, J. L. Ferreira, J. Lubian, and L. F. Canto, Phys. Rev. C **102**, 064628 (2020).
[38] J. Lubian, J. L. Ferreira, J. Rangel, M. R. Cortes, and L. F. Canto, Phys. Rev. C **105**, 054601 (2022).
[39] J. L. Ferreira, J. Rangel, J. Lubian, and L. F. Canto, Phys. Rev. C **107**, 034603 (2023).
[40] H. Kumawat, V. Jha, V. V. Parkar, B. J. Roy, S. Santra, V. Kumar, D. Dutta, P. Shukla, L. M. Pant, A. K. Mohanty *et al.*, Phys. Rev. C **81**, 054601 (2010).
[41] L. C. Chamon, D. Pereira, M. S. Hussein, M. A. Candido Ribeiro, and D. Galetti, Phys. Rev. Lett. **79**, 5218 (1997).
[42] L. C. Chamon, B. V. Carlson, L. R. Gasques, D. Pereira, C. De Conti, M. A. G. Alvarez, M. S. Hussein, M. A. Cândido Ribeiro, E. S. Rossi Jr., and C. P. Silva, Phys. Rev. C **66**, 014610 (2002).
[43] I. J. Thompson, Comput. Phys. Rep. **7**, 167 (1988).
[44] F. Pühlhofer, Nucl. Phys. A **280**, 267 (1977).
[45] V. V. Parkar, S. K. Pandit, A. Shrivastava, R. Palit, K. Mahata, V. Jha, K. Ramachandran, S. Gupta, S. Santra, S. K. Sharma *et al.*, Phys. Rev. C **98**, 014601 (2018).
[46] A. Gavron, Phys. Rev. C **21**, 230 (1980).
[47] O. Tarasov and D. Bazin, Nucl. Instrum. Methods Phys. Res., Sect. B **266**, 4657 (2008).
[48] B. A. Brown and W. D. M. Rae, Nucl. Data Sheets **120**, 115 (2014).
[49] L. F. Canto, P. R. S. Gomes, J. Lubian, L. C. Chamon, and E. Crema, J. Phys. G **36**, 015109 (2009).
[50] L. F. Canto, P. R. S. Gomes, J. Lubian, L. C. Chamon, and E. Crema, Nucl. Phys. A **821**, 51 (2009).
[51] C. Beck, N. Keeley, and A. Diaz-Torres, Phys. Rev. C **75**, 054605 (2007).
[52] F. Souza, N. Carlin, C. Beck, N. Keeley, A. Diaz-Torres, R. Liguori Neto, C. Siqueira-Mello, M. de Moura, M. Munhoz, R. Oliveira *et al.*, Nucl. Phys. A **834**, 420c (2010).
[53] F. Souza, N. Carlin, C. Beck, N. Keeley, A. Diaz-Torres, R. Liguori Neto, C. Siqueira-Mello, M. de Moura, M. Munhoz, R. Oliveira *et al.*, Eur. Phys. J. A **44**, 181 (2010).
[54] V. A. B. Zagatto, B. R. Gonçalves, and D. R. M. Junior, Phys. Rev. C **107**, 044604 (2023).
[55] National Nuclear Data Center, Brookhaven National Laboratory, 2018, http://www.nndc.bnl.gov/.
[56] T. Kibédi, A. B. Garnsworthy, and J. L. Wood, Prog. Part. Nucl. Phys. **123**, 103930 (2022).
[57] B. Paes, G. Santagati, R. M. Vsevolodovna, F. Cappuzzello, D. Carbone, E. N. Cardozo, M. Cavallaro, H. García-Tecocoatzi, A. Gargano, J. L. Ferreira *et al.*, Phys. Rev. C **96**, 044612 (2017).
[58] L. Coraggio, A. Covello, A. Gargano, and N. Itaco, Phys. Rev. C **89**, 024319 (2014).